VALIDATION OF SEISMIC DESIGN PROVISIONS FOR DIAPHRAGMS AND ASSESSMENT OF HIGHER-MODE RESPONSES ON EARTHQUAKE-RESISTANT BUILDINGS – SECOND PROJECT UPDATE

C. Franco Mayorga and Georgios Tsampras

Department of Structural Engineering
University of California San Diego

Abstract

This paper disseminates the ongoing research conducted for the assessment of the Alternative Design Provisions for Diaphragms in buildings per ASCE/SEI 7-22 Section 12.10.3 by utilizing recorded strong-motion acceleration data. Details of the workflow developed for the assessment of the design provisions are presented.

Introduction

Floor diaphragms and their connections to the vertical elements of the seismic force-resisting systems (SFRS) are critical components of earthquake-resistant buildings. Underestimating the level of seismic-induced horizontal forces to which the diaphragms are subjected could be catastrophic. The loss of the ability of the connections of diaphragms to transfer forces to the SFRS could lead to local collapse of the floor or complete collapse of the building. Diaphragm collapses were observed after the Northridge earthquake due to the loss of connections between floor diaphragms and the vertical elements of precast concrete buildings and the vertical elements of tilt-up-wall buildings (Fleischman et al. (2013), Iverson and Hawkins (1994), Tilt-up-Wall Buildings (1996)). After the 2010-2011 Christchurch earthquakes, excessive damage and collapse of floor diaphragms were attributed to inadequate integrity of the load path, underestimation of seismic-induced horizontal forces, and poorly understood interactions between floor diaphragms and walls, supporting beams, and reinforced concrete (RC) moment frames (Gonzalez et al. (2017), Scarry (2014), Kam et al. (2011)). The complex interactions between diaphragms and other structural elements result in unpredictable seismic responses of buildings which often lead to damage to structural members that are designed to remain undamaged (Kam et al. (2011), Bull (2004), Wallace et al. (2012), Henry et al. (2017)).

Earthquake numerical simulations of buildings have shown that the seismic-induced horizontal forces in floor diaphragms can be large relative to the strength of the floor diaphragms. These excessive forces can lead to an inelastic and potentially non-ductile response of the diaphragms (Fleischman and Farrow (2001)). The contribution of the second and higher-mode responses to the total dynamic response of buildings (termed higher-mode effects) may contribute to the excessive forces and floor total accelerations (Sewell et al. (1986), Chopra (2007)). It has been shown that high floor accelerations due to the higher-mode effects can be expected in buildings with SFRS that develop a flexural yield mechanism at the base, such as flexural-dominant RC structural walls (Chopra (2007), Priestley and Amaris (2002), Wiebe sand

Christopoulos (2009), Panagiotou and Restrepo (2009), Tsampras et al. (2016)).

The Alternative Design Provisions for Diaphragms per ASCE/SEI 7-22 (2021) Section 12.10.3 provides estimates of the seismic-induced horizontal forces that can be used to design floor diaphragms. These force estimates were developed based on analysis of experimental data from shaking table tests (Panagiotou et al. (2011), Chen et al. (2016)) and earthquake numerical simulations (Choi et al. (2008), Fleischman (2013)). These force estimates consider the higher-mode effects. Thus, it is expected that they should result in more accurate estimates of the seismic-induced horizontal forces for the design of floor diaphragms.

The California Strong Motion Instrumentation Program (CSMIP) funds projects that utilize recorded acceleration response data to validate the seismic design provisions. In response to the Request for Proposal No. 1020-005 in 2020, Tsampras submitted a proposal that aimed to validate the seismic design provisions for diaphragms and assess the higher-mode responses on earthquake-resistant buildings by utilizing strong-motion acceleration data available in the Center for Engineering Strong Motion Data (CESMD). In 2022, CSMIP awarded a grant, and Tsampras and Mayorga initiated their research toward assessing the design provisions. Mayorga and Tsampras (2022) presented their first progress report during the 2022 Strong Motion Instrumentation Seminar (SMIP). More specifically, the authors focused on the estimation of the location of the center of rigidity from the recorded response data and the comparison between the peak floor accelerations at the estimated center of rigidity and the design acceleration coefficients computed using the equations in ASCE/SEI 7-22 Section 12.10.3.

The preliminary analysis showed that most of the building stations have not been subjected to ground motions with intensities comparable to the design-level earthquake intensity since they were instrumented. In support of this statement, Figure 1 shows the ratios of the peak floor accelerations PFA_x over the design acceleration coefficients C_{px} at three different locations over the height of multiple building stations (i.e., $h_x/h_n = 0.4$, 0.8, and 1.0) with respect to the ratios of the ground motion spectral accelerations at the first-mode period $S_a(T_1, h_x/h_n = 0.0) = S_a(T_1)$ over the design spectral accelerations at the first-mode period $S_{ad}(T_1)$. The figure shows that most of the seismic events resulted in ratios $S_a(T_1)/S_{ad}(T_1)$ below 0.5. The results shown in Figure 1 indicate a lack of recorded acceleration response data from seismic events that result in spectral demands close to the design-level earthquake spectral demand. This introduces two challenges. The first challenge is that the acceleration coefficients need to be at the earthquake intensity of the recorded ground motions to compare them with the peak floor accelerations recorded at the building stations. The second challenge is that the inelastic response of the building stations subjected to the recorded ground motions is limited, therefore, the values of the redaction factor R and overstrength factor Ω_0 need to be adjusted according to the level of inelastic response at which the building stations were subjected. The ongoing research presented in this paper shows how these challenges can be addressed.

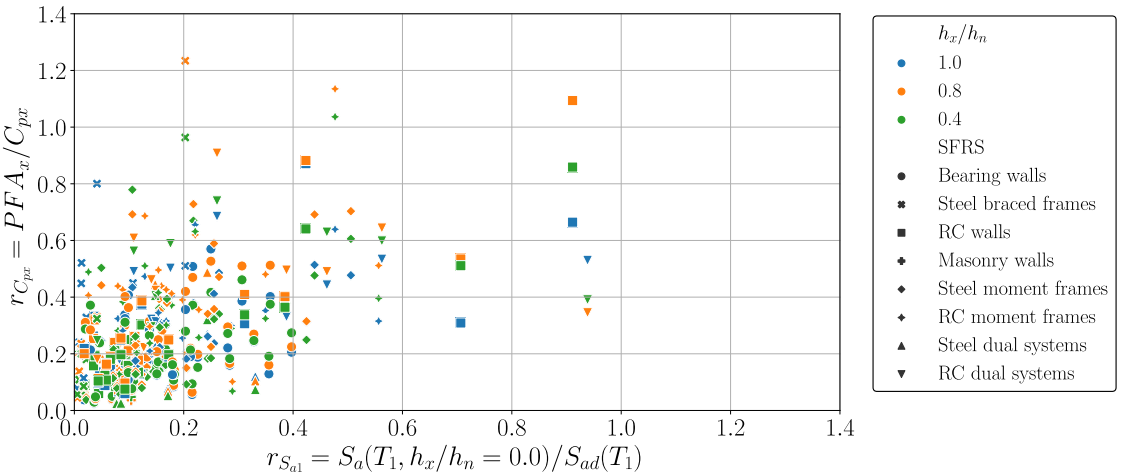

Figure 1. Ratio of the peak floor accelerations over design acceleration coefficients at three different locations over the height of the building stations subjected to various seismic events with respect to the ratio of the ground motion spectral acceleration over the design spectral acceleration at the first-mode period

The objective of this paper is to disseminate the ongoing research toward the validation of the seismic design provisions for diaphragms and assessment of the higher-mode responses on earthquake-resistant buildings by utilizing strong motion acceleration data available in the CESMD. This paper presents a summary of the equations used to compute the design acceleration coefficients per ASCE/SEI 7-22 Section 12.10.3, a workflow including the calculations required for the assessment of the design provisions, estimates of the first-, second-, and third-mode periods, estimates of the seismic performance factors R and Ω_0 based on the peak roof drift obtained from the recorded response data, four scaling approaches for the design acceleration coefficients, and a comparison between the design-based modified acceleration coefficients and the measured peak floor accelerations over the height of the buildings.

Data and metadata from a larger number of building stations are considered in this paper compared to the building stations considered by Mayorga and Tsampras (2022). Buildings within the California Geological Survey Network (CE) that have been subjected to peak floor accelerations larger than 0.2g without restriction on the number of stories are considered in this analysis.

ASCE/SEI 7-22 Section 12.10.3 Alternative Design Provisions for Diaphragms

In-plane seismic design forces for diaphragms, including chords, collectors, and their connections to the vertical elements are given in Section 12.10.3 Alternative Design Provisions for Diaphragms of the ASCE/SEI 7-22. The in-plane seismic design forces are defined as

$$F_{px} = \frac{C_{px}}{R_s} w_{px} \geq 0.2\, S_{DS} I_e w_{px} \tag{1}$$

where C_{px} is the design acceleration coefficient at level x, w_{px} is the weight tributary to the diaphragm at level x, R_s is the diaphragm design force reduction factor, S_{DS} is the design, 5% damped, spectral response acceleration parameter at short periods, and I_e is the building

importance factor. The distribution of design acceleration coefficients over the normalized building height is presented in Figure 2. In this figure, N is the number of stories above the base, h_x is the height above the base to the level x, h_n is the vertical distance from the base to the highest level n of the SFRS of the structure, and C_{p0} is the diaphragm acceleration coefficient at the base. C_{p0} is computed as

$$C_{p0} = 0.4 S_{DS} I_e \tag{2}$$

C_{pi} is the diaphragm design acceleration coefficient at 80% of h_n calculated as

$$C_{pi} = \max\left(0.8 C_{p0}, 0.9 \Gamma_{m1} \Omega_0 C_s\right) \tag{3}$$

where $\Gamma_{m1} = 1 + z_s(1 - 1/N)/2$ is the first modal contribution factor, Ω_0 is the overstrength factor, and C_s is the seismic response coefficient in accordance with Section 12.8.1.1 of the ASCE/SEI 7-22. The term C_{pn} is the diaphragm design acceleration coefficient at h_n computed as

$$C_{pn} = \sqrt{(\Gamma_{m1} \Omega_0 C_s)^2 + (\Gamma_{m2} C_{s2})^2} \geq C_{pi} \tag{4}$$

where

$$C_{s2} = \begin{cases} \min\left(\frac{I_e S_{D1}}{0.03(N-1)}, (0.15N + 0.25) I_e S_{DS}, I_e S_{DS}\right), & N \geq 2 \\ 0 & , \; N = 1 \end{cases} \tag{5}$$

is the higher-mode seismic response coefficient and $\Gamma_{m2} = 0.9 z_s (1 - 1/N)^2$. N was previously defined and z_s is the mode shape factor defined in Section 12.10.3.2.1 of the ASCE/SEI 7-22.

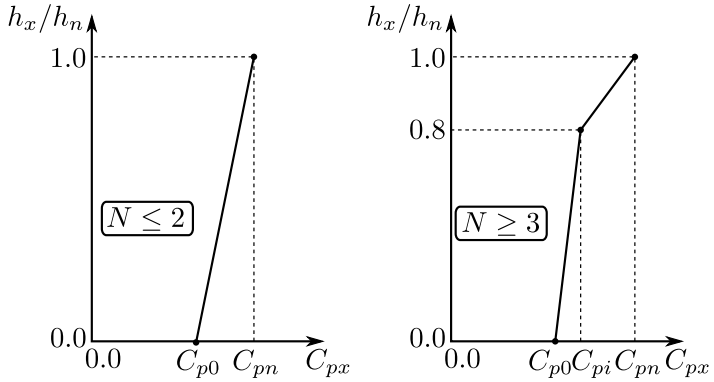

Figure 2. Calculation of the design acceleration coefficients in buildings with N ≤ 2 and in buildings with N ≥ 3 (Figure 12.10-2 in ASCE/SEI 7-22)

Equation (5) considers that the periods of the higher modes probably lie on the ascending, constant, or first descending branch of the two-period design response spectrum given by ASCE/SEI 7-22.

Workflow for Analysis of Recorded Data and Metadata

A workflow for the analysis of the recorded data and metadata to assess the seismic design provisions for diaphragms has been developed using the open-source programming language Python (Van Rossum and Drake (2009)). This workflow allows us to analyze data and metadata available in the CESMD along with metadata that we have generated and appended to the existing datasets. Seventy-seven combinations of building stations and seismic events have been analyzed using the workflow.

The workflow in its current form is executed in sixteen steps. Figure 3 shows a schematic representation of these steps with application to one example building station. Each step in the analysis workflow shown in the figure is summarized as follows:

- Step 1: The data and metadata are loaded into the workflow. The loaded database includes information available on the CESMD database along with information that has been manually extracted from drawings and other sources available for the building stations, their sites, and seismic events.
- Step 2: For the analysis of a specific building station under the selected seismic events indicated in the information incorporated in Step 1, the analyst selects the building station of interest. Analysis of the data and metadata of all building stations loaded in Step 1 can be performed as well.
- Step 3: A database is created within Python using Pandas DataFrames (type of database variable in Python).
- Step 4: The recorded accelerations for each channel are plotted and saved for checking purposes.
- Step 5: The peak recorded accelerations for each channel are computed and plotted over the height of the building station for checking purposes.
- Step 6: The location of the center of rigidity at each sufficiently instrumented floor is estimated using the method proposed by Şafak and Çelebi (1990) along with the utilization of the recorded acceleration data (Mayorga and Tsampras (2022)). Plots of the coherence area, a measure of the correlation between the translational and torsional responses, with respect to the estimated position of the center of rigidity in the floor plan are provided for the selected seismic events. If multiple seismic events are available, the potential shift of the estimated location of the center of rigidity can be computed from the derived data.
- Step 7: The estimation of the center of rigidity using recorded data allows the decomposition of the floor displacement, velocity, and acceleration data to horizontal translational and torsional floor displacements, velocities, and accelerations. The accuracy of the estimation of the location of the center of rigidity determines the accuracy of the decomposition of the translational and torsional components of the recorded floor displacements, velocities, and accelerations.
- Step 8: The spectral accelerations at instrumented floors are computed for the selected seismic events. The results are compared with the metadata already available in the CESMD for checking purposes.
- Step 9: The first-mode translational periods in the two directions of the building station are estimated considering the SFRS (based on metadata added manually in the expanded database), the building height, and the peak ground velocity using the empirical equations

derived by Xiang at al. (2016). See Section "Estimation of First-, Second- and Third-mode Periods".

- Step 10: The second- and third-mode translational periods are computed based on the estimated first-mode period using the analytical equations derived by Miranda and Taghavi (2005). See Section "Estimation of First-, Second- and Third-mode Periods".
- Step 11: The design spectrum for the specific building station is computed along with the design spectral accelerations and ground motion spectral accelerations at first-, second-, and third-mode translational periods of the building station in two horizontal directions. The ratio of the ground spectral acceleration over the design spectral accelerations at each period is also computed and stored in the expanded database as additional metadata.
- Step 12: The design acceleration coefficients for the two translational directions of the building station are computed using the design equations per ASCE/SEI 7-22 Section 12.10.3. The design acceleration coefficients are also computed using the design equations per ASCE/SEI 7-22 Section 12.10.1. for comparison purposes.
- Step 13: The distribution of the translational components of the recorded peak floor accelerations over the height of the building station is compared with the distribution of the design acceleration coefficients over the height of the building station.
- Step 14: R and Ω_0 at the earthquake intensity of the measured ground motions are estimated based on the peak roof drift at the center of rigidity computed using the displacement time-histories given in the CESMD dataset. See Section "Estimation of Seismic Performance Factors".
- Step 15: The design acceleration coefficients are scaled to the measured (recorded) earthquake intensity using four scaling approaches. See Section "Design-based Modified Acceleration Coefficients".
- Step 16: Metrics to quantify the difference in magnitude and distribution over the building height of the design-based modified acceleration coefficients and the peak floor accelerations are computed. See Section "Preliminary Comparison between Scaled Acceleration Coefficients and Measured Peak Floor Accelerations".

Buildings Stations

A set of seventy-seven instrumented buildings that are part of the CSMIP were selected to compare their peak floor accelerations to the design acceleration coefficients. The building stations considered in this analysis belong to the California Geological Survey Network (CE). They have various numbers of stories, mostly below 20 stories. They were designed for risk categories II or IV. Their foundation soils were classified as B, C, or D. They have been subjected to ground motions that resulted in recorded peak floor accelerations larger than 0.2g since they were instrumented.

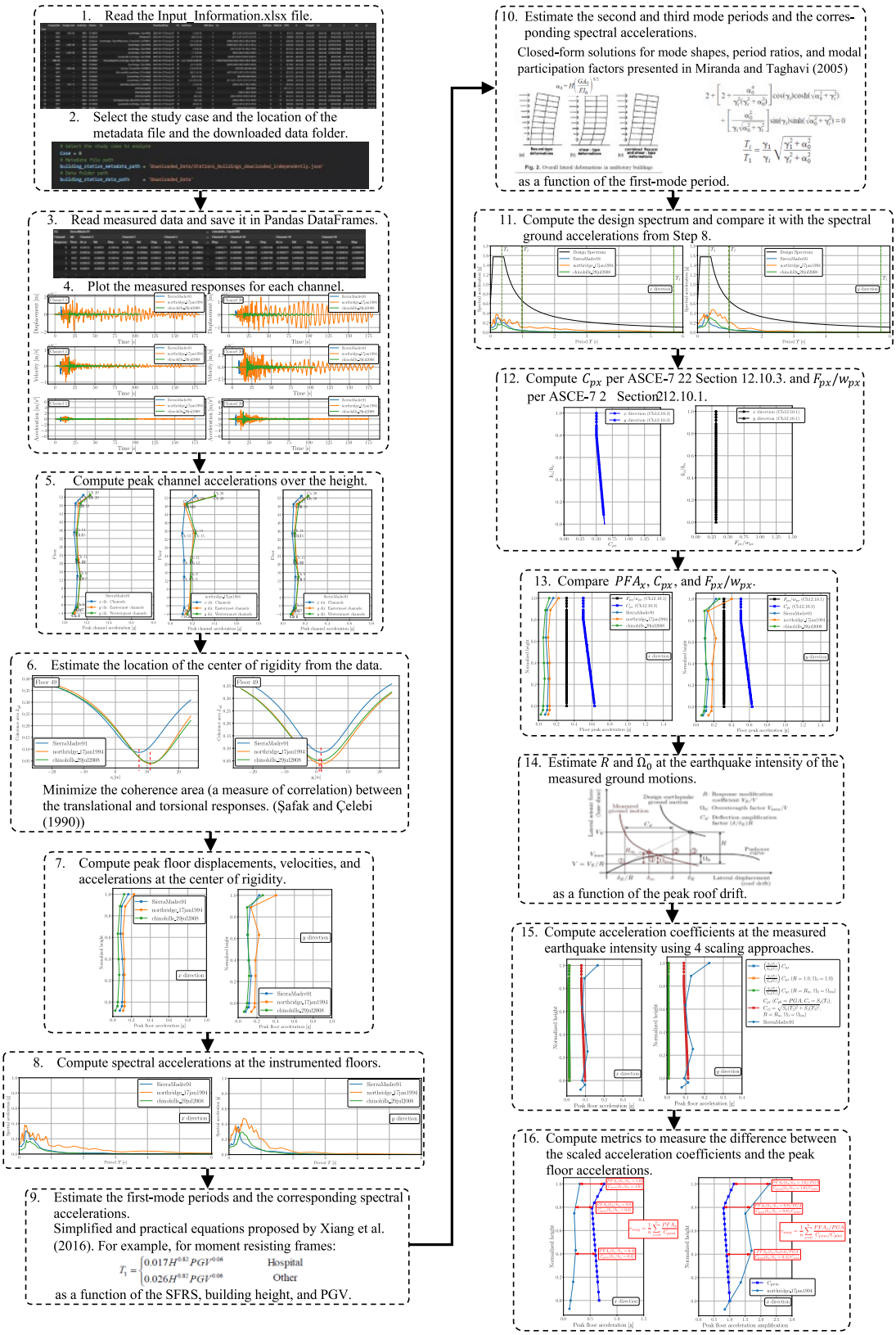

Figure 3. Schematic representation of the workflow and application to one example building station

Forty-three cases of analysis, each of which corresponds to one building station and one or more seismic events, are considered. Table 1 lists the station of measurement, recorded seismic events, design date, design code, number of stories, building risk category, site class, spectral response acceleration parameter at short periods S_s, and spectral response acceleration parameter at a period of 1 [s] S_1 for each analysis case. These spectral response acceleration parameters are obtained based on the building location in terms of latitude and longitude given on the CESMD website https://www.strongmotioncenter.org/ and the risk category defined in terms of the building use or occupancy.

Table 1. Analysis case, station of measurement, recorded seismic event, design date, design code, number of stories, building risk category, site class, spectral response acceleration parameter at short periods S_s, and spectral response acceleration parameter at a period of 1 [s] S_1

Case	Station	Recorded seismic events	Design date	Design code**	Number of stories*	Risk Category	Site Class	S_s[g] *****	S_1[g] *****
1	CE14654	Northridge (1994)	1985	UBC-82	14	II	D	1.851	0.652
2	CE24236	Whittier (1987)	1925	--	14	II	D	2.092	0.750
3	CE24322 ***	Northridge (1994), Encino (2014)	1964	--	13	II	D	1.962	0.700
4	CE24464	Northridge (1994)	1967	LABC-66	20	II	C	2.082	0.747
5	CE24566	Northridge (1994)	1971	--	12	II	C	2.090	0.762
6	CE24569	Northridge (1994)	1961	LABC-60	15	II	C	1.993	0.710
7	CE24601	Landers (1992), Northridge (1994)	1980	--	17	II	C	1.978	0.705
8	CE24602	Sierra Madre (1991), Northridge (1994), Chino Hills (2008)	1988-90	--	52	II	C	1.967	0.700
9	CE24643	Northridge (1994)	1967	--	19	II	D	2.082	0.744
10	CE24680	Encino (2014)	1965	LABC-64	14	II	D	2.270	0.720
11	CE57357 ****	Mt. Lewis (1986), Loma Prieta (1989)	1972	--	13	II	D	1.530	0.523
12	CE58480	Loma Prieta (1989)	1964	--	18	II	D	1.500	0.600
13	CE58483	Loma Prieta (1989)	1964	--	24	II	C	1.802	0.686
14	CE58639	Berkeley (2018)	1975	UBC-73	13	II	D	1.865	0.711
15	CE12266	Palm Springs (1986)	1970	--	1	II	D	2.122	0.856
16	CE12284	Palm Springs (1986)	1974	--	4	II	D	1.500	0.610
17	CE12299	Palm Springs (1986)	1967	--	4	IV	D	1.814	0.754
18	CE13213	Borrego Springs (2010)	1994	--	3	IV	D	1.773	0.694
19	CE13589	Landers (1992), Northridge (1994)	1971	--	10	IV	D	1.384	0.494
20	CE14311	Whittier (1987)	1968	--	5	II	D	1.546	0.556
21	CE14606	Northridge (1994), Chino Hills (2008), Whittier Narrows (2010)	1984	UBC-83	8	II	D	1.842	0.657
22	CE23285	Landers (1992), Northridge (1994)	1968	--	5	II	D	2.384	1.014
23	CE23287	Landers (1992), Northridge (1994), San Bernardino (2009), Borrego Springs (2010)	1970	--	6	II	D	2.438	0.977
24	CE23495	Palm Springs (1986), Landers (1992), Big Bear (1992), Cabazon (2018), ci38457511 (2019)	1971	--	1	II	D	1.890	0.744

Case	Station	Recorded seismic events	Design date	Design code**	Number of stories*	Risk Category	Site Class	S_s[g] *****	S_1[g] *****
25	CE23511	Chino Hills (2008)	1971	--	2	II	D	1.762	0.639
26	CE23516	Landers (1992)	1983	--	3	II	D	2.453	0.983
27	CE24385	Whittier (1987), Sierra Madre (1991), Northridge (1994)	1974	--	10	II	D	2.017	0.699
28	CE24386	Northridge (1994)	1965	--	7	II	D	2.115	0.712
29	CE24517	Landers (1992)	1974	--	3	II	D	1.500	0.600
30	CE24571	Sierra Madre (1991), Landers (1992)	1963	--	9	II	C	2.090	0.761
31	CE24571 ******	Northridge (1994)	1963	--	9	II	C	2.090	0.761
32	CE24609	Landers (1992), Northridge (1994), ci38443183 (2019), ci38457511 (2019)	1986	UBC-79	5	IV	D	1.500	0.600
33	CE57355	Morgan Hill (1984), Loma Prieta (1989), Alum Rom (2007)	1964	--	10	II	D	1.500	0.600
34	CE57356	Morgan Hill (1984), Loma Prieta (1989), Alum Rock (2007)	1971	--	10	II	D	1.500	0.600
35	CE58334	Piedmont (2007), Berkeley (2011), Piedmont (2015)	1973	--	3	II	B	2.161	0.834
36	CE13698	Lake Elsinore (2007), Chino Hills (2008)	1991	--	2	II	D	2.024	0.797
37	CE23634	Landers (1992), Big Bear (1992), Northridge (1994)	1991	--	5	IV	D	2.287	0.914
38	CE24104	Chatsworth (2007)	1983	--	2	IV	D	2.055	0.724
39	CE24248	ci38695658 (2020)	1986	--	9	IV	C	2.287	0.914
40	CE24370	Whittier (1987)	1976	--	6	II	D	2.023	0.694
41	CE24463	Whittier (1987), Northridge (1994)	1970	LABC-70	5	II	D	1.898	0.676
42	CE24514	Whittier (1987), Northridge (1994)	1976	--	6	IV	C	2.653	0.857
43	CE47459	Morgan Hill (1984), Loma Prieta (1989)	1948 & 1955	--	4	II	D	2.588	0.967

* Number of stories above the ground level
** Design code given in the building station websites. UBC: Uniform Building Code. LABC: Los Angeles Building Code.
*** The building was strengthened with friction dampers after the 1994 Northridge Earthquake.
**** 96 dampers were installed after the Loma Prieta Earthquake to reduce building movement.
***** S_s and S_1 are obtained based on the building location and Risk Category.
****** Building station CE24571 was divided into two analysis cases because the data from Channel 7 on the second floor was not found for the seismic events associated with the analysis case 30.

The SFRS for the analysis cases given in Table 1 are assumed based on the design date (and design code when available). Bearing walls, Steel braced frames, RC walls, Masonry walls, Steel moment frames, RC moment frames, Steel dual systems, and RC dual systems are considered. The dual systems are SFRS composed of a combination of walls or braced frames and moment frames where the moment frames can resist at least 25% of the prescribed seismic forces.

Table 2 lists the assumed SFRS, the corresponding response modification coefficient R, overstrength factor Ω_0, and the deflection amplification factor C_d. The seismic performance

factors R, Ω_0, and C_d are obtained from ASCE/SEI 7-22 Table 12.2-1.

Table 2. Assumed seismic force-resisting systems, response modification coefficients R, overstrength factors Ω_0, and deflection amplification factor C_d

Case	Assumed Seismic Force-resisting System (SFRS) in x and y directions*	Response modification coefficient R in x and y directions	Overstrength factor Ω_0 in x and y directions	Deflection amplification factor C_d in x and y directions
1	Steel dual systems	6.0	2.5	5.0
2	RC dual systems	5.5	2.5	4.5
3	RC moment frames	5.0	3.0	4.5
4	RC moment frames	5.0	3.0	4.5
5	Steel moment frames	4.5	3.0	4.0
6	Steel moment frames	4.5	3.0	4.0
7	Bearing walls	4.0	2.5	4.0
8	Steel braced frames	6.0	2.0	5.0
9	Steel moment frames, Steel braced frames	4.5, 6.0	3.0, 2.0	4.0, 5.0
10	RC dual systems	5.5	2.5	4.5
11	Steel moment frames	4.5	3.0	4.0
12	Steel moment frames	4.5	3.0	4.0
13	RC dual systems	5.5	2.5	4.5
14	Bearing walls	4.0	2.5	4.0
15	Bearing walls	1.5	2.5	1.5
16	RC walls	5.0	2.5	4.5
17	Steel moment frames	4.5	3.0	4.0
18	Steel moment frames	4.5	3.0	4.0
19	RC walls	5.0	2.5	4.5
20	Bearing walls	4.0	2.5	4.0
21	Bearing walls	3.5	2.5	2.25
22	RC walls	5.0	2.5	4.5
23	Bearing walls	4.0	2.5	4.0
24	Bearing walls	4.0	2.5	4.0
25	RC moment frames	5.0	3.0	4.5
26	Steel moment frames	4.5	3.0	4.0
27	RC dual systems	5.5	2.5	4.5
28	RC dual systems	5.5	2.5	4.5
29	Masonry walls	2.0	2.5	2.0
30	RC moment frames	5.0	3.0	4.5
31	RC moment frames	5.0	3.0	4.5
32	Steel moment frames	4.5	3.0	4.0
33	RC moment frames, RC walls	5.0	3.0, 2.5	4.5
34	Bearing walls	4.0	2.5	4.0
35	RC walls	5.0	2.5	4.5
36	Steel dual systems	6.0	2.5	5.0
37	Steel moment frames	4.5	3.0	4.0
38	Steel moment frames	4.5	3.0	4.0
39	Steel braced frames	8.0	2.0	4.0
40	Steel moment frames	4.5	3.0	4.0
41	RC moment frames	5.0	3.0	4.5
42	RC walls	5.0	2.5	4.5
43	RC walls	5.0	2.5	4.5

* The SFRS are assumed based on the definitions given in Table 12.2-1 of the ASCE/SEI 7-22.

Estimation of First-, Second-, and Third-mode Periods

The first-mode translational periods in the two directions of the building stations are estimated using the empirical equations proposed by Xiang et al. (2016). They identified the modal quantities (i.e., natural periods and equivalent viscous damping ratios) of ninety-four building stations using three time-domain and one frequency-domain system identification methods considering more than one thousand seismic records. They combined the results from these system identification methods to obtain unique values of the first-mode period and damping ratio for each combination of building station and seismic event. They proposed simplified and practical equations for the first-mode period and damping ratio in terms of structural system type, building height, and peak ground velocity. The equations are used to estimate the first-mode period for each combination of building station and seismic event listed in Table 1. The assumed SFRS given in Table 2, the building heights obtained from the building station websites, and the recorded peak ground velocities are considered as inputs for the equations proposed by Xiang et al. (2016).

The second- and third-mode periods are estimated using the analytical equations derived by Miranda and Taghavi (2005). They used a simplified model based on an equivalent continuum structure consisting of a combination of a flexural beam and a shear beam to approximate the dynamic characteristics of buildings. Assuming uniform distributions of mass and stiffness over the height of the building, they presented the following closed-form solution for the period ratios

$$\frac{T_i}{T_1} = \frac{\gamma_1}{\gamma_i}\sqrt{\frac{\gamma_1^2+\alpha_0^2}{\gamma_i^2+\alpha_0^2}} \tag{6}$$

where T_i is the ith-mode period, γ_i is the eigenvalue parameter associated with the ith-mode period, and α_0 is a nondimensional parameter that controls the degree of participation of the overall flexural and overall shear deformations to the total deformation in the simplified models of multistory buildings. γ_i is the ith-root of the characteristic equation

$$2 + \left[2 + \frac{\alpha_0^4}{\gamma_i^2(\gamma_i^2+\alpha_0^2)}\right] cos(\gamma_i)\cosh\left(\sqrt{\gamma_i^2+\alpha_0^2}\right) + \frac{\alpha_0^2}{\gamma_i\sqrt{\gamma_i^2+\alpha_0^2}} sin(\gamma_i)\sinh\left(\sqrt{\gamma_i^2+\alpha_0^2}\right) = 0 \tag{7}$$

and α_0 usually ranges from 0 to 1.5 for shear wall and braced frame buildings, from 1.5 to 5 for dual system buildings, and from 5 to 20 for moment-resisting frame buildings (Miranda and Reyes (2002)).

Equation (6) is used to estimate the second- and third-mode periods for each combination of building station and seismic event listed in Table 1. Values of α_0 equal to 0.75 for shear wall and braced frame buildings, 3.25 for dual system buildings, and 12.5 for moment-resisting frame buildings are assumed (Miranda and Reyes (2002), Taghavi and Miranda (2005)).

Estimation of Seismic Performance Factors

The definition of the seismic performance factors R and Ω_0 used to compute the design acceleration coefficients per ASCE/SEI 7-22 Section 12.10.3 assumes that buildings are subjected to a design-level earthquake intensity ground motion. Most of the building stations considered in this study were subjected to ground motions with an earthquake intensity lower than the design level. Thus, the acceleration coefficients must be computed using ASCE/SEI 7-22 considering R and Ω_0 values modified to account for the reduced intensity of ground motions. The computed acceleration coefficients can be compared with the recorded peak floor accelerations. This section presents a simplified and practical way to estimate R and Ω_0 based on the peak roof drift computed at the estimated center of rigidity as a measure of the level of inelastic response of the building.

The seismic performance factors are defined in terms of the global inelastic response of the SFRS idealized as the pushover curve presented in Figure 4. This figure is based on Figure 1-1 in FEMA P695 (2009), in which R, Ω_0, and C_d are represented as incremental differences despite they are dimensionless ratios of forces, accelerations, or displacements. In Figure 4, V_E represents the force that would be developed in the SFRS if the system remained entirely linear-elastic for the design-level earthquake ground motion. V_{max} represents the actual maximum strength of the fully yielded system, and V is the seismic base shear required for design. R and Ω_0 are defined as

$$R = \frac{V_E}{V} \tag{8}$$

and

$$\Omega_0 = \frac{V_{max}}{V} \tag{9}$$

, respectively. δ_E represents the roof drift of the SFRS corresponding to V_E, δ_E/R represents the roof drift of the SFRS corresponding to V, and δ represents the roof drift of the SFRS corresponding to the design-level earthquake ground motion assuming that the system has reached the plastic range. C_d is defined as

$$C_d = \frac{\delta}{\delta_E} R \tag{10}$$

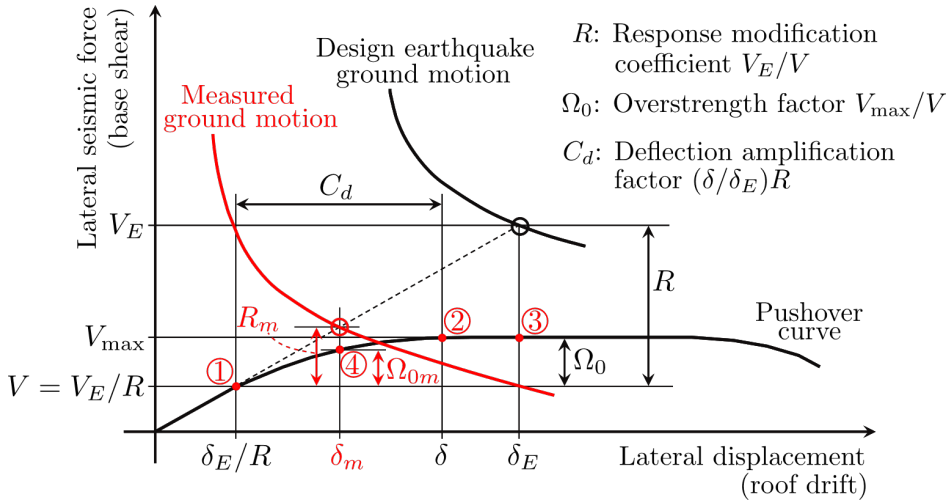

Figure 4. Illustration of seismic performance factors (R, Ω_0, and C_d)

For a measured (recorded) ground motion with an intensity lower than the design-level earthquake, the relationship of the expected base shear demand and the expected roof drift demand is represented by the red curve in Figure 4. The seismic performance factors R_m and Ω_{0m} at the measured roof drift δ_m (point 4) are lower than the R and Ω_0 expected for the design-level earthquake ground motion (point 3), respectively. Considering that the pushover curve is a property of the system, R_m varies between 1.0 when $\delta_m = \delta_E/R$ and R when $\delta_m = \delta_E$ (variation between points 1 and 3), and Ω_{0m} varies between 1.0 when $\delta_m = \delta_E/R$ and Ω_0 when $\delta_m = \delta$ (variation between points 1 and 2). Assuming that the deformation of the building follows the first-mode translational shape, the roof drift of the yielded building corresponding to the design-level earthquake ground motion is equal to the design upper limit or allowable story drift Δ_a given in ASCE/SEI 7-22 Table 12.12-1 for $h_{sx} = h_n$ (i.e., $\delta = \Delta_a$), and a linear variation of R_m and Ω_{0m} in terms of δ_m, the seismic performance factors for a measured ground motion can be estimated as

$$R_m = \begin{cases} 1.0, & \delta_m < \frac{\delta_E}{R} = \frac{\Delta_a}{C_d} \\ 1.0 + \frac{(R-1.0)}{\Delta_a/C_d(R-1.0)}(\delta_m - \Delta_a/C_d), & \frac{\Delta_a}{C_d} \le \delta_m < \frac{\Delta_a}{C_d}R \\ R, & \delta_m \ge \delta_E = \frac{\Delta_a}{C_d}R \end{cases} \tag{11}$$

and

$$\Omega_{0m} = \begin{cases} 1.0, & \delta_m < \frac{\delta_E}{R} = \frac{\Delta_a}{C_d} \\ 1.0 + \frac{(\Omega_0-1.0)}{\Delta_a(1.0-1/C_d)}(\delta_m - \Delta_a/C_d), & \frac{\Delta_a}{C_d} \le \delta_m < \Delta_a \\ \Omega_0, & \delta_m \ge \Delta_a \end{cases} \tag{12}$$

, respectively.

The authors acknowledge that this approach assumes that either the allowable roof drift controls the design or it is close to the roof drift corresponding to the design-level earthquake ground motion assuming that the system has reached the plastic range. The authors also acknowledge that the variation of the overstrength factor in terms of the roof drift is not linear. However, it is considered a practical approximation of R_m and Ω_{0m} used to compute the design acceleration coefficients per ASCE/SEI 7-22 Section 12.10.3 for measured ground motions with earthquake intensities different to the design-level earthquake intensity considering multiple building stations with various SFRS. The authors will continue the assessment of the assumptions during the remaining duration of the ongoing project.

Design-based Modified Acceleration Coefficients

The design acceleration coefficients are modified to consider the earthquake intensity of the measured ground motions. Four scaling approaches are used to modify the design acceleration coefficients. The design-based modified acceleration coefficients are compared with the peak floor accelerations at the center of rigidity induced by the measured ground motions.

Approach 1

This approach considers the design acceleration coefficients per ASCE/SEI 7-22 Section 12.10.3 scaled with respect to the ratio of the ground motion spectral acceleration over the design spectral acceleration at the estimated first-mode period ($S_a(T_1)/S_{ad}\ (T_1)$). This approach represents a case in which the design acceleration spectrum is scaled by $S_a(T_1)/S_{ad}\ (T_1)$ assuming the R and Ω_0 corresponding to a building behaving in the plastic range.

Approach 2

This approach considers the design acceleration coefficients per ASCE/SEI 7-22 Section 12.10.3 using $R = 1.0$ and $\Omega_0 = 1.0$ scaled with respect to the ratio of the ground motion spectral acceleration over the design spectral acceleration at the estimated first-mode period ($S_a(T_1)/S_{ad}\ (T_1)$). This approach represents a case in which the design acceleration spectrum is scaled by $S_a(T_1)/S_{ad}\ (T_1)$ assuming the R and Ω_0 corresponding to a building behaving in the linear-elastic range.

Approach 3

This approach considers the design acceleration coefficients per ASCE/SEI 7-22 Section 12.10.3 using $R = R_m$ and $\Omega_0 = \Omega_{0m}$ scaled with respect to the ratio of the ground motion spectral acceleration over the design spectral acceleration at the estimated first-mode period ($S_a(T_1)/S_{ad}\ (T_1)$). This approach represents a case in which the design acceleration spectrum is scaled by $S_a(T_1)/S_{ad}\ (T_1)$ assuming the R and Ω_0 corresponding to a building with an inelastic response depending on the earthquake intensity of the measured ground motion.

Approach 4

This approach considers the design acceleration coefficients per ASCE/SEI 7-22 Section

12.10.3 using $C_{p0} = S_a(T = 0.0\ [s]) = PGA$, $C_s = S_a(T_1)$, $C_{s2} = \sqrt{(S_a(T_2)^2 + S_a(T_3)^2)}$, $R = R_m$, and $\Omega_0 = \Omega_{0m}$. This approach represents a case in which the design acceleration spectrum is modified in scale and shape taking into account the ground motion spectral accelerations at $T = 0\ [s]$ and at the first-, second-, and third-mode periods assuming the R and Ω_0 corresponding to a building with an inelastic response depending on the earthquake intensity of the measured ground motion.

The first two scaling approaches represent extreme cases in terms of the level of inelastic response of the building stations. The third scaling approach includes the level of inelastic response based on the roof drift at the center of rigidity. The fourth scaling approach incorporates the shape of the ground motion spectral accelerations. The next section compares the magnitude and distribution over the building height of the design-based modified acceleration coefficients computed using the four scaling approaches with the peak floor accelerations at the center of rigidity from the measured ground motions.

Preliminary Comparison between Design-based Modified Acceleration Coefficients and Measured Peak Floor Accelerations

The design-based modified acceleration coefficients introduced in the previous section are compared with the peak floor accelerations at the center of rigidity for each combination of building station and seismic event listed in Table 1. The magnitude and distribution over the building height of the design-based acceleration coefficients are compared with the magnitude and distribution over the building height of the peak floor accelerations at the center of rigidity.

The average ratio of the peak floor accelerations (PFA_x) over the design-based modified acceleration coefficients (C_{pxm}) through the floors of the building (i.e., $r_{mag} = (1/n)\sum_{x=0}^{n} PFA_x/C_{pxm}$) is used as a metric to quantify the difference in magnitude between the design-based modified acceleration coefficients and the peak floor accelerations. r_{mag} larger than 1.0 indicates that the design-based modified acceleration coefficients underestimate the peak floor accelerations and r_{mag} lower than 1.0 indicates the design-based modified acceleration coefficients overestimate the peak floor accelerations.

The average ratio of the amplification of the peak floor accelerations (PFA_x/PGA; PGA: peak ground acceleration) over the amplification of the design-based modified acceleration coefficients (C_{pxm}/C_{p0m}) through the floors of the building (i.e., $r_{amp} = (1/n)\sum_{x=0}^{n}[(PFA_x/PGA)/(C_{pxm}/C_{p0m})]$ is used as a metric to quantify the difference in the distribution over the height of the building between the design-based modified acceleration coefficients and the peak floor accelerations. r_{amp} larger than 1.0 indicates that the design-based modified acceleration coefficients underestimate the amplification of the peak floor accelerations and r_{amp} lower than 1.0 indicates that the design-based modified acceleration coefficients overestimate the amplification of the peak floor accelerations over the height of the building.

Figure 5 shows r_{mag} and r_{amp} in terms of the SFRS for each combination of building station and seismic events listed in Table 1 and the SFRS listed in Table 2. The four scaling approaches are shown in the figure. Each circular marker corresponds to one direction of

analysis (x or y) for one combination of building station and seismic event. The blue markers correspond to the scaling approach 1, the orange markers correspond to the scaling approach 2, the green markers correspond to the scaling approach 3, and the red markers correspond to the scaling approach 4. The square white markers correspond to mean values of r_{mag} and r_{amp} for each SFRS and scaling approach. The mean values and coefficients of variation of r_{mag} and r_{amp} are presented in Table 3 and Table 4, respectively. These tables also include the count of combinations of building stations and seismic events considering each direction of analysis as an independent data point. The last rows of Table 3 and Table 4 correspond to the mean values and coefficients of variations of r_{mag} and r_{amp}, respectively, considering all the SFRS.

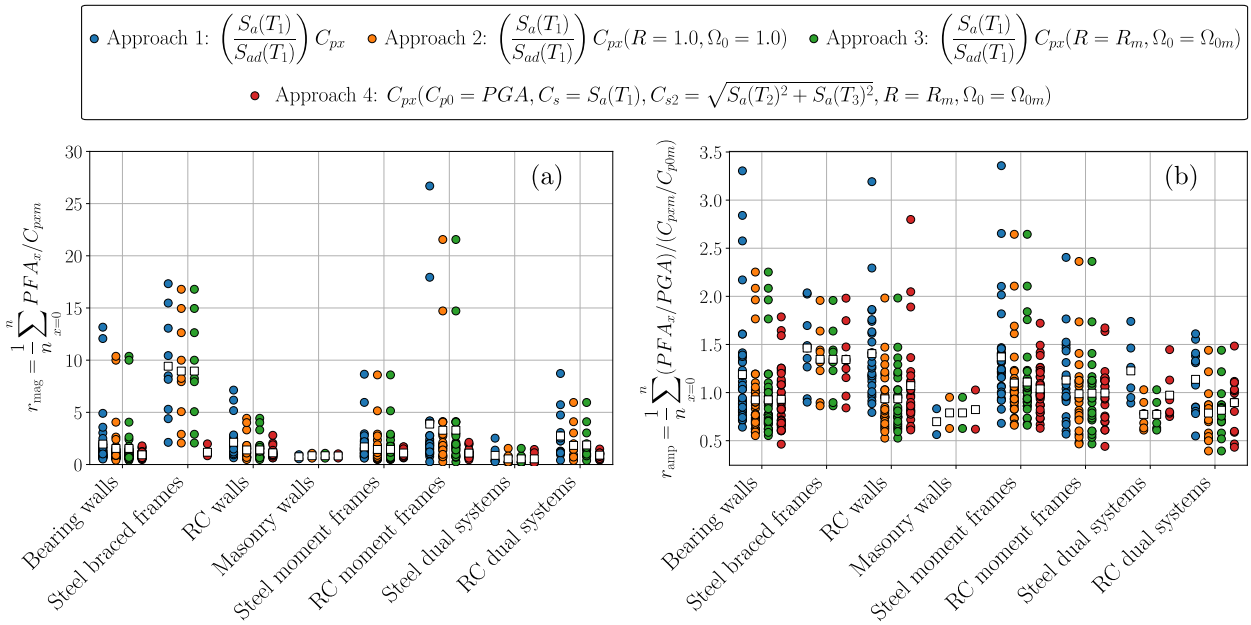

Figure 5. r_{mag} and r_{amp} ratios in terms of the SFRS for each combination of building station and seismic events listed in Table 1 and the SFRS listed in Table 2. Design-based modified acceleration coefficients using four scaling approaches

Table 3. Mean values and coefficients of variation of the r_{mag} ratios

SFRS	Count	Mean value $\mu_{r_{mag}}$ (coefficient of variation $\sigma_{r_{mag}}/\mu_{r_{mag}}$ [%])			
		Approach 1	Approach 2	Approach 3	Approach 4
Bearing walls	40	1.95 (134.5)	1.54 (137.4)	1.54 (137.4)	0.93 (32.9)
Steel Braced frames	9	9.42 (54.6)	8.95 (57.6)	8.95 (57.6)	1.18 (27.6)
RC walls	27	2.13 (75.3)	1.40 (72.2)	1.40 (72.2)	1.12 (41.2)
Masonry walls	2	0.75 (37.4)	0.84 (39.1)	0.84 (39.1)	0.82 (35.0)
Steel moment frames	35	1.69 (91.9)	1.44 (106.6)	1.45 (106.0)	1.11 (25.0)
RC moment frames	23	3.87 (156.7)	3.28 (149.9)	3.29 (149.3)	1.09 (40.4)
Steel dual systems	6	0.88 (103.9)	0.54 (101.1)	0.54 (101.1)	0.54 (107.6)
RC dual systems	14	2.74 (83.2)	1.83 (85.0)	1.87 (81.6)	0.90 (32.8)
All	156	2.65 (136.9)	2.16 (147.7)	2.16 (147.1)	1.02 (37.5)

Almost all the design-based modified acceleration coefficients using the scaling approach 2 resulted in the same r_{mag} and r_{amp} that those obtained using the scaling approach 3. This

suggests that most of the building stations behaved in the linear-elastic or near to the linear-elastic range ($R_m \approx 1.0$ and $\Omega_{0m} \approx 1.0$) when they were subjected to the ground motions generated by the seismic events considered in this stage of the ongoing project. This is expected because most of the measured ground motions are lower in intensity than the design-level earthquake.

Figure 5a) and Table 3 shows that the design-based modified acceleration coefficients using the scaling approaches 1, 2, and 3 underestimate the magnitude of the peak floor accelerations. The mean values of the corresponding r_{mag} are larger than 2.0 with coefficients of variations larger than 130.0% for these scaling approaches. This suggests that scaling the design acceleration coefficients by the ratio $S_a(T_1)/S_{ad}(T_1)$ is not a good approach to estimate the magnitude of peak floor accelerations even if the level of inelastic response is well estimated. The design-based modified acceleration coefficients using the scaling approach 4 approximate reasonably well the magnitude of the peak floor accelerations. The mean value of r_{mag} is 1.02 with a coefficient of variation of 37.5% for this scaling approach. Considering the SFRS with more than 10 data points, the scaling approach 4 better estimates the magnitude of the peak floor accelerations for Bearing walls (r_{mag} closer to 1.0 with a coefficient of variation of 32.9%) and worse estimates the magnitude of the peak floor accelerations for the RC walls (r_{mag} further from 1.0 with a coefficient of variation of 29.6%), but still being a reasonable approximation.

Figure 5a) also shows that r_{mag} for some of the Steel braced frames and RC moment frames using the scaling approaches 1-3 are larger than 15.0, which means that the magnitude of the peak floor accelerations is severely underestimated using these scaling approaches.

Table 4. Mean values and coefficients of variation of the r_{amp} ratios

SFRS	Count	Mean value $\mu_{r_{amp}}$ (coefficient of variation $\sigma_{r_{amp}}/\mu_{r_{amp}}$ [%])			
		Approach 1	Approach 2	Approach 3	Approach 4
Bearing walls	40	1.19 (41.9)	0.92 (38.1)	0.92 (38.1)	0.93 (28.3)
Steel Braced frames	9	1.46 (29.5)	1.35 (25.4)	1.35 (25.4)	1.34 (28.7)
RC walls	27	1.41 (34.7)	0.94 (33.7)	0.94 (33.7)	1.07 (43.4)
Masonry walls	2	0.70 (33.8)	0.79 (36.5)	0.79 (36.5)	0.82 (46.5)
Steel moment frames	35	1.37 (36.1)	1.10 (34.6)	1.11 (35.4)	1.04 (22.3)
RC moment frames	23	1.13 (33.5)	0.99 (40.0)	0.99 (39.4)	1.00 (27.2)
Steel dual systems	6	1.23 (25.0)	0.77 (20.2)	0.77 (20.2)	0.97 (30.4)
RC dual systems	14	1.14 (27.2)	0.79 (34.9)	0.82 (31.5)	0.90 (29.8)
All	156	1.26 (39.8)	0.98 (39.8)	0.98 (39.6)	1.01 (33.6)

Figure 5b) and Table 4 shows that the distribution of the design-based modified acceleration coefficients over the heights of the buildings approximate reasonably well the distribution of the peak floor accelerations over the heights of the buildings. The mean values of the corresponding r_{amp} are in between 0.98 and 1.26 with coefficients of variations smaller than 40.0% for the scaling approaches considered in this analysis. Considering the SFRS with more than 10 data points, the scaling approach 4 better estimates the distribution of the peak floor accelerations over the height of the buildings for RC moment frames (r_{amp} closer to 1.0 with a coefficient of variation of 27.2%) and worse estimates the distribution of the peak floor accelerations over the height of the buildings for the RC dual systems (r_{amp} further from 1.0 with a coefficient of variation of 33.6%), but still being a good approximation.

The authors are evaluating the implementation of other metrics to compare the acceleration coefficients computed based on the design provision equations and the measured peak floor accelerations.

Conclusions

The analysis of the results of the ongoing project presented in this document suggests that:

- The equations to compute the design acceleration coefficients per ASCE/SEI 7-22 Section 12.10.3 can predict reasonably well the magnitude of the peak floor accelerations when the spectral accelerations of the measured ground motions at $T = 0\ [s]$ and at the first-, second-, and third-mode periods are considered. The scaling approaches that considered only the spectral accelerations of the measured ground motions at the first-mode periods underestimate the peak floor accelerations.

- The equations to compute the design acceleration coefficients per ASCE/SEI 7-22 Section 12.10.3 can predict reasonably well the distribution of the peak floor accelerations over the height of the building. However, measured data or simulated data at the design-level earthquake intensity is required to fully validate the design provisions.

Acknowledgments

The authors acknowledge the California Strong Motion Instrumentation Program for the financial support through the project called "Validation of Seismic Design Provisions for Diaphragms and Assessment of Higher-Mode Responses on Earthquake-Resistant Buildings" and the Chilean National Agency for Research and Development (ANID) for the financial support through the foreign doctoral scholarship 2020. Any opinions, findings, and conclusions expressed in this paper are those of the authors and do not necessarily reflect the views of others acknowledged here.

References

ASCE/SEI 7-22 (2021). Minimum design loads and associated criteria for buildings and other structures. *American Society of Civil Engineers*.

Bull, D. K. (2004). Understanding the Complexities of Designing Diaphragms in Buildings for Earthquakes. *Bulletin of the New Zealand Society for Earthquake Engineering* 37, no. 2: 70–88. https://doi.org/10.5459/bnzsee.37.2.70-88.

Chen, Michelle C., Pantoli, E., Wang, X., Astroza, R., Ebrahimian, H., Hutchinson, T.C., Conte, J.P., Restrepo, J. I., Marin, C., Walsh, K. D., Bachman, R.E., Hoehler, M.S., Englekirk, R., and Faghihi, M. (2016). "Full-Scale Structural and Nonstructural Building System Performance

during Earthquakes: Part I – Specimen Description, Test Protocol, and Structural Response." *Earthquake Spectra* 32, no. 2: 737–70. https://doi.org/10.1193/012414eqs016m.

Choi, H., Christopoulos, C., and Tremblay, R. (2008). Comparison of the Seismic Response of Steel Buildings Incorporating Self-Centering Energy Dissipative Braces, Buckling Restrained Braced and Moment Resisting Frames. Research Report 05-2008, University of Toronto, Canada.

Chopra, Anil K (2007). *Dynamics of Structures*. Pearson Education.

Federal Emergency Management Agency (FEMA) (2009). FEMA P695 Recommended Methodology for Quantification of Building System Performance and Response Parameters. *Project ATC-63*, Prepared by the Applied Technology Council, Redwood City.

Fleischman, R. B., and Farrow, K. T. (2001). Dynamic Behavior of Perimeter Lateral-System Structures with Flexible Diaphragms. *Earthquake Engineering & Structural Dynamics* 30, no. 5: 745–63. https://doi.org/10.1002/eqe.36.

Fleischman, R. B., Restrepo, J. I., Naito, C. J., Sause, R., Zhang, D., and Schoettler, M. (2013). "Integrated Analytical and Experimental Research to Develop a New Seismic Design Methodology for Precast Concrete Diaphragms." *Journal of Structural Engineering* 139, no. 7: 1192–1204. https://doi.org/10.1061/(ASCE)ST.1943-541X.0000734.

González, Alfredo, Spacone, E., and Nascimbene, R. (2017). Performance-Based Seismic Design Framework for RC Floor Diaphragms in Dual Systems. *Procedia Engineering*, X International Conference on Structural Dynamics, EURODYN 2017, 199: 3546–51. https://doi.org/10.1016/j.proeng.2017.09.512.

Henry, Richard S., Dizhur, D., Elwood, K. J., Hare, J., and Brunsdon, D (2017). Damage to Concrete Buildings with Precast Floors during the 2016 Kaikoura Earthquake. *Bulletin of the New Zealand Society for Earthquake Engineering* 50, no. 2: 174–86. https://doi.org/10.5459/bnzsee.50.2.174-186.

Iverson, J. K., and Hawkins, N. M. (1994). Performance Of Precast/Prestressed Building Structures During Northridge Earthquake. *PCI Journal* 39, no. 2. https://trid.trb.org/view/390643.

Kam, W. Y., Pampanin, S., and Elwood, K. (2011). Seismic Performance of Reinforced Concrete Buildings in the 22 February Christchurch (Lyttleton) Earthquake. *University of Canterbury. Civil and Natural Resources Engineering*. https://ir.canterbury.ac.nz/handle/10092/9006.

Mayorga, C.F., and Tsampras. G., (2022). Validation of seismic design provisions for diaphragms and assessment of higher-mode responses on earthquake-resistant buildings. *Strong Motion Instrumentation Program Seminar*, Department of Conservation, California.

Miranda E., and Reyes C.J. (2002). Approximate lateral drift demands in multistory buildings with nonuniform stiffness. *ASCE Journal of Structural Engineering* 128, no. 7: 840–849 https://doi.org/10.1061/(ASCE)0733-9445(2002)128:7(840).

Miranda E., and Taghavi S. (2005). Approximate floor acceleration demands in multistory buildings I: Formulation. *ASCE Journal of Structural Engineering* 131, no. 2: 203–211 https://doi.org/10.1061/(ASCE)0733-9445(2005)131:2(203).

Panagiotou, Marios, and Restrepo, J. I. (2009). Dual-Plastic Hinge Design Concept for Reducing Higher-Mode Effects on High-Rise Cantilever Wall Buildings. *Earthquake Engineering & Structural Dynamics* 38, no. 12: 1359–80. https://doi.org/10.1002/eqe.905.

Panagiotou, Marios, Restrepo, J. I., and Conte, J. P. (2011). Shake-Table Test of a Full-Scale 7-Story Building Slice. Phase I: Rectangular Wall. *Journal of Structural Engineering* 137, no. 6: 691–704. https://doi.org/10.1061/(ASCE)ST.1943-541X.0000332.

Priestley, M. J., and Alejandro D. Amaris (2002). *Dynamic Amplification of Seismic Moments and Shear Forces in Cantilever Walls*. IUSS Press.

Şafak, Erdal, and Çelebi, M (1990). Method to Estimate Center of Rigidity Using Vibration Recordings. *Journal of Structural Engineering* 116, no. 1: 85–97. https://doi.org/10.1061/(ASCE)0733-9445(1990)116:1(85).

Scarry, J M (2014). Floor Diaphragms – Seismic Bulwark or Achilles' Heel. *NZSEE Conference*, Auckland, New Zealand.

Sewell, R. T., Cornell, C. A., Toro, G. R., and McGuire, R. K. (1986). A Study of Factors Influencing Floor Response Spectra in Nonlinear Multi-Degree-of-Freedom Structures. *John A. Blume Earthquake Engineering Center Technical Report Series*. https://purl.stanford.edu/vf765pj9489.

Tilt-up-Wall Buildings. (1996). *Earthquake Spectra* 12, no. 1 (suppl): 99–123. https://doi.org/10.1193/1.1585922.

Taghavi, S. and Miranda, E. (2005). Approximate Floor Acceleration Demands in Multistory Buildings. II: Applications. *Journal of Structural Engineering* 131, no. 2: 212–220. https://doi.org/10.1061/(ASCE)0733-9445(2005)131:2(212).

Tsampras, Georgios, Sause, R, Zhang, D., Fleischman, R. B, Restrepo, J. I., Mar, D., and Maffei, J. (2016). Development of Deformable Connection for Earthquake-Resistant Buildings to Reduce Floor Accelerations and Force Responses. *Earthquake Engineering & Structural Dynamics* 45, no. 9: 1473–94. https://doi.org/10.1002/eqe.2718.

Van Rossum, G., and Drake, F. L. (2009). Python 3 Reference Manual. Scotts Valley, CA: CreateSpace.

Wallace, John W., Massone, L. M., Bonelli, P., Dragovich, J., Lagos, R., Lüders, C., and Moehle, J. (2012). Damage and Implications for Seismic Design of RC Structural Wall Buildings. *Earthquake Spectra* 28, no. 1(supl): 281–99. https://doi.org/10.1193/1.4000047.

Wiebe, L., and Christopoulos, C. (2009). Mitigation of Higher Mode Effects in Base-Rocking Systems by Using Multiple Rocking Sections. *Journal of Earthquake Engineering* 13, no. sup1: 83–108. https://doi.org/10.1080/13632460902813315.

Xiang, Yijun, Harris, A., Naeim, F., and Zareian, F. (2016). Identification And Validation of Natural Periods and Modal Damping Ratios for Seismic Design and Building Code. *SMIP16 Seminar Proceedings*.